Nonlinear Finite Element Analysis of Steel Fibers Reinforced Post-Tensioned Lightweight Concrete Beams

Ayman H. H. Khalil[1], Ashraf M. A. Heniegal[2] and, Mohammed Mahmoud Attia[3]

[1.] Professor, Department of Structural Engineering, Ain Shams University, Cairo, Egypt
[2.] Professor, Department of Structural Engineering, Suez University, Suez, Egypt
[3.] Assistant Lecturer, Department of Civil Constructions and Architecture, Suez University, Suez, Egypt
[1]ayman.hussien.khalil@eng.asu.edu.eg, [2]ashraf_henigal@yahoo.com, [3]mohammed_mahmoed2011@yahoo.com

Abstract: This paper presents a nonlinear finite element modeling (FEM) and analysis of post-tensioned fibrous lightweight concrete beams made of natural pumice that subjected to static bending load until failure. Nine post-tensioned lightweight simple beams were modeled using ANSYS nonlinear finite element software. The main parameters studies were the volume fractions of discrete steel fibers (DSF) and a partial prestressing ratio (PPR), where the volume fractions of DSF varied of 0% to 1.5%, and PPR varied of 60% to 90%. It was found that the ratio between the FEM to the experimental results of the cracking load, yielding load and ultimate load varies from 0.89 to 1.30, 0.93 to 1.05 and 1 to 1.05 respectively. It was clear that the results of FEM gave similar results to the experimental behavior.

[Ayman H. H. Khalil, Ashraf M. A. Heniegal, and Mohammed Mahmoud Attia, **Nonlinear Finite Element Analysis of Steel Fibers Reinforced Post-Tensioned Lightweight Concrete Beams.** *N Y Sci J* 2018;11(6): 80-92]. ISSN 1554-0200 (print); ISSN 2375-723X (online). http://www.sciencepub.net/newyork. 12. doi:10.7537/marsnys110618.12.

Keywords: A nonlinear finite element analysis; Ansys; Post-tensioned; Partial prestressing ratio; Steel fibers; Pumice lightweight aggregate; Lightweight concrete.

1. Introduction

Improvement of calculation methods and analysis of the behavior of reinforced concrete by, either creating a model on a computer or counting with analytical calculation methods are used extensively in recent years. The behavior of a reinforced concrete element is generally observed by conducting the experiment on laboratory environment, but this process considerably takes up much time [1]. The studies are limited due to the problems in providing the materials and the proper conditions to conduct the experiments and scarcity of usage of materials which are constituted according to certain size and number of elements. Modeling of all these processes unlimitedly in the computer is dependent on the capacity of the computer being used. While modeling on the computer, properties and limit conditions of materials should be defined properly and completely [2]. ANSYS finite element program is chosen for this study. Finite element method is a numeric method which can solve complex and difficult physical problems with an acceptable approximation. As concrete is a material showing nonlinear behavior during loading, it is modeled in such a way that it will show a nonlinear behavior with ANSYS finite element program [3]. Prestressed concrete is a form of reinforced concrete that gather the advantage of the strengths of steel and concrete that has many usages such as buildings, power station and numerous types of bridge systems, but high self-weight and low ductility of prestressed concrete members are the most problems that face its application [4,5,6]. Lightweight concrete has many properties such as thermal and acoustic insulation besides low self-weight and the most common way to produce it is obtained by using lightweight aggregate to produce structural lightweight aggregate concrete (SLWAC) that its problems are weakness and brittleness of lightweight aggregate [7,8]. SLWAC is usually defined as a concrete with an oven dry density of no greater than 2000 kg/m³ compared with that of 2400 kg/m³ for normal weight concrete (NWC) [9,10]. Steel fibers are short, discontinuous, an aspect ratio, length to the equivalent diameter, from 20:100 with several cross-sections, and small enough to spars randomly in a fresh concrete mix by using conventional mixing procedures [11,12]. Fibers enhance the mechanical performance of concrete regarding its tensile and flexural, shear strength, toughness, and ductility. So, steel fiber overcomes the defect of lightweight prestressed with ductility [13,14]. On the other hand, the uniform dispersion of DSF throughout the concrete provided isotropic strength properties which are not exhibited by conventionally reinforced concrete [15].

2. Research Objective

The objective of this paper is to study the behavior of the post-tensioned lightweight steel fibers reinforced concrete beams using three-dimensional finite element analysis. For this purpose, nine post-tensioned lightweight beams with and without DSF were obtained by using finite element solutions of ANSYS program. The experimental and FEM results are compared numerically and graphically.

3. Experimental Study

Figure 1 shows the beams' geometry, supports arrangement, internal reinforcement and strand profile of the tested specimens. The experimental program includes nine post-tensioned simple beams with R-shape cross-section. Eight of them were of fibrous reinforced lightweight concrete, while one of them was of normal reinforced lightweight concrete. All beams had the same overall dimensions with total length 2500 mm, an overall height of 350 mm, overall width 200 mm and clear spans of 2250 mm. The strand profiles were kept the same for all beams and were symmetrical about midspan of the beams. All the prestressing strands included seven wires with nominal diameters of 15.24 mm and ultimate tensile strength of 1860 N/mm². All beams reinforced with two bars bottom steel each of them 12 mm diameter. The top reinforcement of all beams was two bars of diameter 10 mm. The stirrups in all beams consisted of 2 vertical branches of 10 mm diameter steel bars that were spaced at 140 mm, to prevent shear failure. All Non-prestressing steel have yield stress 520 N/mm². All steel reinforcements had a nominal modulus of elasticity Es =200 GPa.

The specimens were divided into four groups according to the PPR and the volume fraction of the DSF, as shown table 1. ***Group one*****;** includes three specimens B1, B2, and B3 and have DSF 0%, 0.5% and 1% of the concrete volume respectively. Specimens in this group were having one strand with 60% PPR. ***Group two*****;** includes three specimens B4, B5, B6, and have DSF 0.5%, 1%, and 1.5%, of the concrete volume respectively. Specimens in this group were having two strands with 80% PPR. ***Group three*****;** includes two specimens, B7, B8 and have DSF 1% and 1.5% of the concrete volume respectively. Specimens in this group were having three strands with 85% PPR. ***Group four*****;** includes one specimen B9 and have DSF 1.5% of the concrete volume. Specimen in this group was having four strands with 90% PPR. The PPR defined via the following equation [16]:

$$PPR = (ApsFpy) / (ApsFpy + AsFy) \quad (1)$$

Where; Aps, the area of the prestressing steel. Fp*y*, the yielding in the prestressing steel. A*s*, the area of the non-prestressed tension steel. F*y* the yielding of the non-prestressed tension steel.

Table 1: Summary of beam`s details

Numbers of			ID Beams	PPR %	Discrete steel fiber %				Bottom *steel*	Stirrup *steel*
Beams	Group	Strand			0.0	0.5	1.0	1.5		
1	One	1	B1	60	■				2Ø 12	Ø10@140 mm
2			B2			■				
3			B3				■			
4	Two	2	B4	80		■				
5			B5				■			
6			B6					■		
7	Three	3	B7	85			■			
8			B8					■		
9	Four	4	B9	90				■		

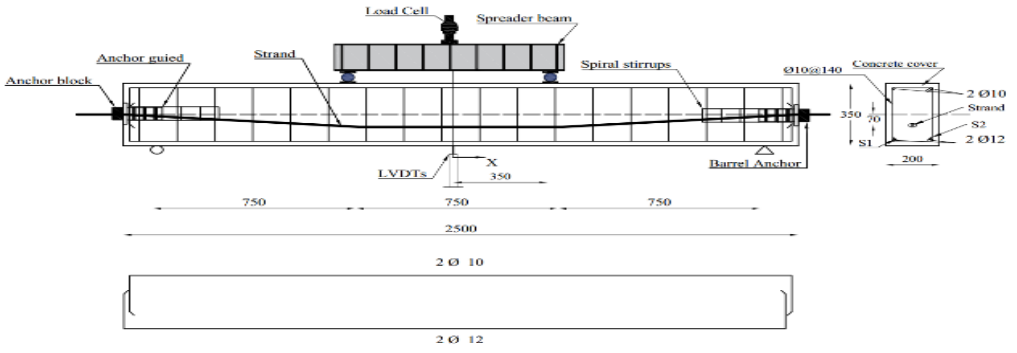

Fig. 1: Typical details and internal steel strain gauges' locations for all beams

The used material was; Cement (CEM I 42.5) [17], Natural sand, Crushed dolomite, Natural pumice lightweight aggregate coarse [18], End Hook steel fiber that has the average length 45 mm, the average thickness 1 mm and the aspect ratio 45, Fy 1100 N/mm². Table 2 shows the unite weight, cube strength and splitting tensile strength for all mixes. For each tested beams, deflections were measured using Linear Variable Distance Transducers (LVDTs) at mid-span beams. Strains in tension

zone were monitored using electrical strain gauges which installed on the internal longitudinal steel bars, of each beams, as indicated in Fig.1. Test setup of beams was; two supports one of them was a hinge of support and the other was roller support, loaded at two points at 350 mm from the mid-span.

Table 2: Results of; unit weight, compressive strength and tensile strength of concrete

Mix No.	steel fiber %				Unit weight	Compressive	Tensile strength
	0.0	0.5	1.0	1.5	Kg/m³	N/mm²	
1					1724.5	35.4	3.6
2					1765.6	37.5	4.2
3					1836.2	39.0	4.9
4					1866.1	40.5	5.8

4. ANSYS FINITE ELEMENT MODEL

The FEM includes modeling beams with the same dimensions and properties of tested beams in experimental work. Due to the symmetry in cross-section of the concrete beams and loading, symmetry was utilized in the FEM, only one quarter of the beam was modeled. There are three alternative techniques are mainly used for modeling reinforcement in a three-dimensional finite element model of a concrete structure; the discrete model, the embedded model, and the smeared model, are shown in figures 2,3,4 [19]. In this study the prestressing and non-prestressing steel is modeled as discrete while the DSF modeled as smeared model techniques.

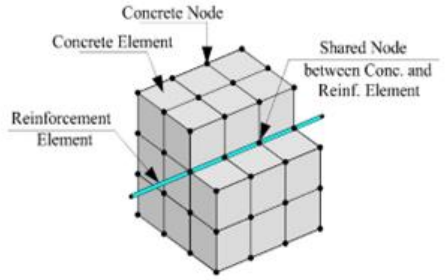

Fig.2: Discrete model [19]

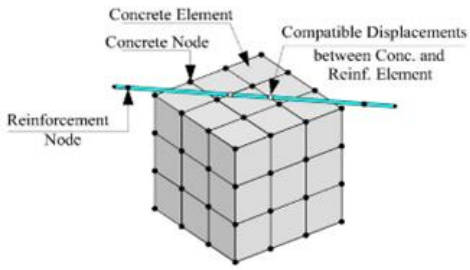

Fig.3: Embedded model [19]

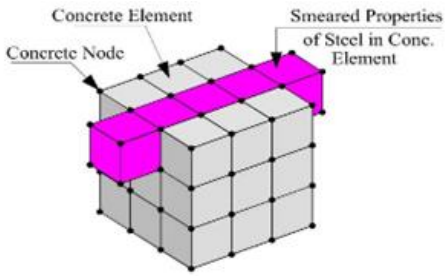

Fig.4: Smeared model [19]

4.1 Defining; element types, real constants, and material properties

a). Element types

A Solid 65 element was used to model the concrete. This element has eight nodes with three degrees of freedom at each node – translations in the nodal x, y, and z directions. This element is capable of plastic deformation, cracking in three orthogonal directions, and crushing, as shown in figure 5 [20].

A Solid 185 element was used for steel plates at the supports for the beams. This element has eight nodes with three degrees of freedom at each node – translations in the nodal x, y, and z directions, as shown in figure 6 [20].

A LINK 180 element was used to model prestressing and non-prestressing steel reinforcement bars. The element is a uniaxial tension-compression element with three degrees of freedom at each node: translations in the nodal x, y, and z directions. This element is also capable of plastic deformation, as shown in figure 7 [20].

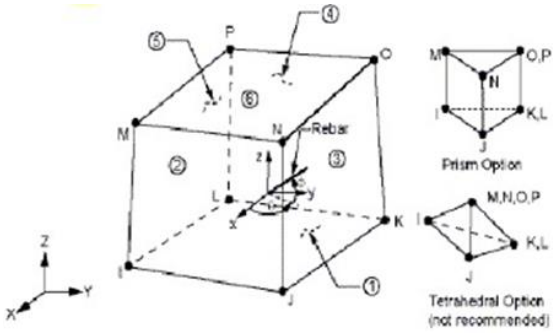

Fig. 5: SOLID 65 [20]

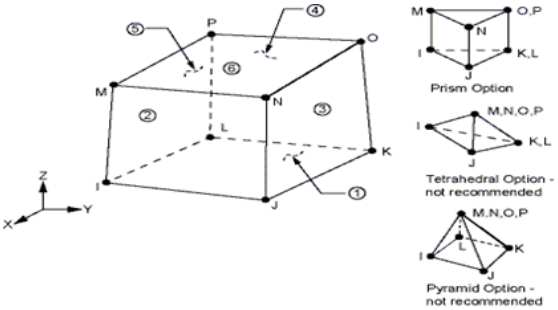

Fig. 6: SOLID185 [20]

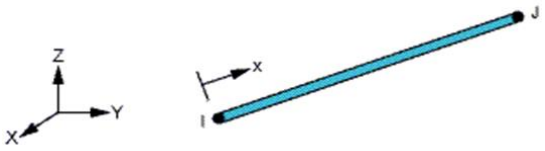

Fig. 7: LINK 180 [20]

b). Real constants

Table 3 shows real constants for all element type. No real constant set for the Solid 185 elements.

Concrete ANSYS 2015, allows to the user to enter three rebar materials in the concrete [20]. Each material corresponds to x, y, and z directions in the element, as shown figure 5.

In case of concrete without DSF, real constants defined only for SOLID 65 element, therefore, all real constants which activate the smeared reinforcement are disabled by putting it equal zero. In case concrete with DSF is formulated in smeared model to represent DSF specifications; including the material number, the volume ratio, and the orientation angles for DSF [20]. The material number refers to the type of material for the DSF. The volume ratio refers to the ratio of the DSF to concrete in the element. The orientation angles refer to the orientation of the DSF in the smeared model.

Prestressing and non-prestressing steel LINK 180 has main real constants that is cross sectional area. Real constants for all steel show in table 3.

Table 3: Real constant of each element type

Element types	Real constant Set*	*Real constant for beam without DSF*				*Real constant for beam with DSF*			
			Real constant for rebar 1	Real constant for rebar 2	Real constant for rebar 3		Real constant for rebar 1	Real constant for rebar 2	Real constant for rebar 3
Solid 65	35	*Material number*	0	0	0	*Material number*	4**	4**	4**
		Volume ratio	0	0	0	*Volume ratio*	*= volume fraction for DSF/3*		
		Orientation angle	0	0	0	*Orientation angle*	0	90	0
		Orientation angle	0	0	0	*Orientation angle*	0	0	90
Link180	10	Cross-sectional area mm²		78.5	Stirrups and top reinforcement				
	12	Cross-sectional area mm²		113.1	Bottom reinforcement				
	140	Cross-sectional area mm²		138.2	Prestressed steel				
Solid185	Solid 185 has no real constant								

*Labeled Number
** Labeled Number of DSF

c). Material properties

Concrete; Parameters needed to define the material models were obtained from experimental study and the literature can be found in table 2,4, respectively. Material model number 1 refers to the Solid 65 elements that required linear isotropic and multilinear isotropic material properties to properly model concrete. The multilinear isotropic material uses the von Mises failure criterion along with the William and Warnke (1974) model to define the failure of the concrete, [21]. EX, is the modulus of elasticity of concrete, and PRXY is the Poisson's ratio was 0.2.

The relation between the static modulus of elasticity and cube compressive strength of lightweight concrete as in Eq.2, [22]:

$$\mathrm{Em} = \left(\frac{\sigma}{2400}\right)^2 * 20000 + .2Fcu \qquad (2)$$

Where; Em, The modulus of elasticity of lightweight concrete in N/mm². Fcu, Cube compressive strength in kg/cm² and $\boldsymbol{\sigma}$, The SLWAC density in kg/m³.

The modulus of elasticity for fibrous lightweight concrete is expressed in Eq. (3), [23]:

$$Ec=Em\ (1+0.173\ Vf\ Lf\ /df) \qquad (3)$$

Where; Ec, The modulus of elasticity of fibrous lightweight concrete in N/mm². Vf, volume fraction of DSF. Lf, Length of DSF and df, Diameter of DSF.

Density was added to the concrete material property, as shown table 2, so the self-weight of the concrete beam could be considered [24]. The shear transfer coefficients for open and closed cracks were determined using the work of Kachlakev, et al. [25] as a basis. Convergence problems occurred when the shear transfer coefficient for the open crack dropped below 0.2. No deviation of the response occurs with the change of the coefficient. Therefore, the coefficient for the open and close crack were set to 0.2, table 4. The uniaxial cracking stress was based upon the modulus of rupture as table 2. The uniaxial crushing stress in this model was based on the uniaxial compressive strength. It was entered as -1 to turn off the crushing capability of the concrete element as suggested by past researchers [25]. Convergence problems have been repeated when the crushing capability was turned on.

Prestressing, non-prestressing steel and DSF; Material model number 2 and 3 refer to the Link 180 element where material model number 2

and 3 refer to non-prestressing steel reinforcement and prestressing steel, respectively. The Link180 element is being used for all the steel reinforcement in the beam and it is assumed to be bilinear isotropic. Bilinear isotropic material is also based on the von Mises failure criteria. The bilinear model requires the yield stress fy. The yield stress was defined as shown in table 4.

On the other hand, material number 4 refer to DSF.

Steel plates and supports; Material model number 5 refers to the Solid 185 elements. The Solid 185 element is being used for the steel plates at loading points and supports on the beam. Therefore, this element is modeled as a linear isotropic element with a modulus of elasticity for the steel Es=200GPa, and Poisson's ratio (0.3).

Table 4: Material models for typical model

Material number*	Element type	Materials properties					
		Linear Isotropic		Multilinear Isotropic		Non-Metal plasticity of concrete	
1	Solid 65	EX	According to Eq 2.3	stress	strain	Open shear transfer coefficient	0.2
		PRXY	0.2	According to Ref. [21]		Closed shear transfer coefficient	0.2
						Uniaxial cracking stress fctr	Table 1
						Uniaxial crushing stress f`c	-1
						Biaxial crushing stress	**
						Hydrostatic pressure	**
						Hydrostatic biaxial crush stress	**
						Hydrostatic uniaxial crush stress	**
						Tensile crack factor	**
2	Link 180	Linear Isotropic		Bilinear Isotropic			
		EX	200 GPa	Yield Stss	520 MPa		
		PRXY	0.3				
3	Link 180	Linear Isotropic		Bilinear Isotropic			
		EX	193 GPa	Yield Stss	1674 MPa		
		PRXY	0.3				
4		Linear Isotropic		Bilinear Isotropic			
		EX	200 GPa	Yield Stss	1100 MPa		
		PRXY	0.3				
5	Solid 185	Linear Isotropic					
		EX	200 GPa				
		PRXY	0.3				

*Labeled number, **Default input data.

4.2 Modeling methodology

The beam, plates, and supports were modeled as volumes, but the prestressing and non-prestressing steel bars were modeled as lines. Since a quarter of the beam is being modeled, the model is 1250 mm long, with a cross-section of 100*350 mm. The dimensions for the concrete volume are shown in table 5. The zero values for the X, Y and Z coordinates coincide with the center of the cross-section for the concrete beam. The 1250 mm dimension for the X-coordinates is the mid-span of the beam. Due to symmetry, only one loading plate and one support plate are needed.

The support is a 50*100*12 mm. Steel plate at the load point is 100*100*12.5 mm. The dimensions for the plate and support are shown in table 5. The combined volumes of the plate, support, and beam are shown in Figure 8. Reinforcement exists at a plane of symmetry and in the beam. The area of steel at the plane of symmetry is one half the normal area for bar because one half of the bar is cut off. Shear stirrups are modeled throughout the beam. Only half of the stirrup is modeled because of the symmetry of the beam as shown figure 9.

Table 5: Dimensions for Concrete, Steel Plate, and Steel Support Volumes

ANSYS	Concrete mm		Steel Plates mm		Steel Support mm	
X1.X2 X-Coordinates	0	1250	825	925	100	150
Y1.Y2 X-Coordinates	0	350	350	362.5	0	-12
Z1.Z2 X-Coordinates	0	100	0	100	0	100

4.3 Meshing

To obtain good results from the Solid 65 elements, the use of a rectangular mesh is recommended. Therefore, the mesh was set-up such that square or rectangular elements were created, as shown figure 9. The volume sweep command was used to mesh the steel plate and support. This properly sets the width and length of elements in the plates to be consistent with the elements and nodes in the concrete portions of the model. The element type number, material number, and real constant set number for the model were set for each mesh, as shown in table 4. The overall mesh; of the concrete, plate, support volumes,

prestressed and non-prestressed reinforcement is shown in figure 9. The necessary element divisions are noted. Maximum meshing dimension for all models is 12.5 x 12.5 mm.

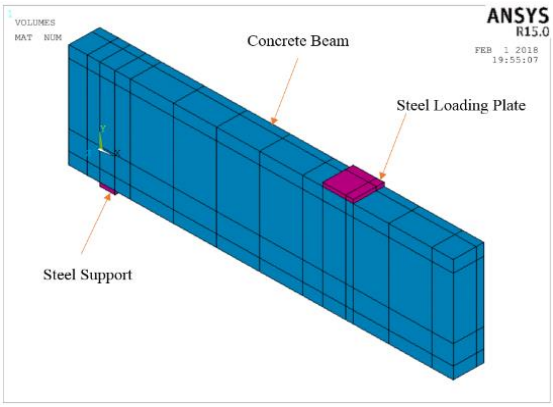

Fig. 8: Volumes Created in ANSYS

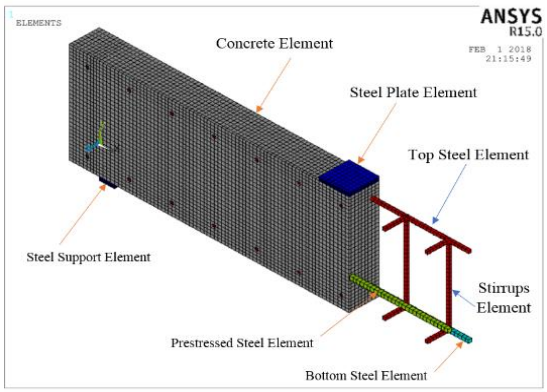

Fig.9: Mesh of beam

4.4 Applied prestressing force on strand

The effect of prestressing force was modeled as initial strain. The initial strain, for real constant set 140 and material number set 3, were determined from the effective prestressed and the modulus of elasticity of prestressing steel. The effective prestressed is the stress in the prestressing steel due to prestressing force after computing all losses.

4.5 Loads and boundary conditions

Displacement boundary conditions are needed to constrain the model to get a unique solution. To ensure that the model acts the same way as the experimental beam, boundary conditions need to be applied at points of symmetry, and where the supports and loadings exist. The symmetry boundary conditions were set first. The model being used is symmetric about two planes. The boundary conditions for both planes of symmetry are shown in figure 10. Nodes defining a vertical plane through the beam cross-section centroid defines a plane of symmetry. To model the symmetry, nodes on this plane must be constrained in the perpendicular direction. These nodes, therefore, have a degree of freedom constraint UX = 0. Second, all nodes selected at Z = 0 define another plane of symmetry. These nodes were given the constraint UZ = 0. The support was modeled in such a way that a roller was created. A single line of nodes on the plate were given constraint in the UY, and UZ directions, applied as constant values of 0. By doing this, the beam will be allowed to rotate at the support. The support condition is shown in Figure 11. The force, P, applied at the steel plate is applied across the entire centerline of the plate. Figure 12 illustrates the plate and applied loading.

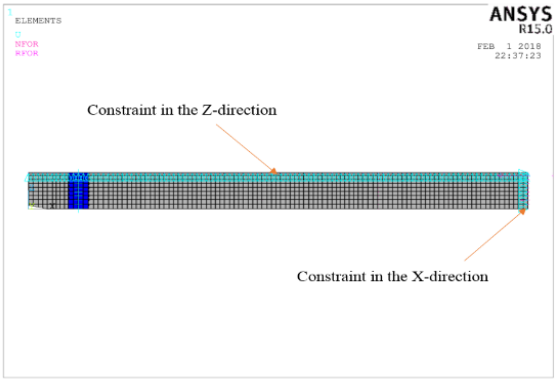

Fig. 10: Boundary conditions for planes of symmetry

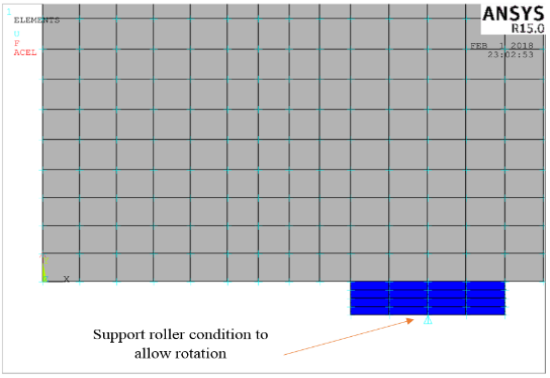

Fig.11: Boundary Condition for Support

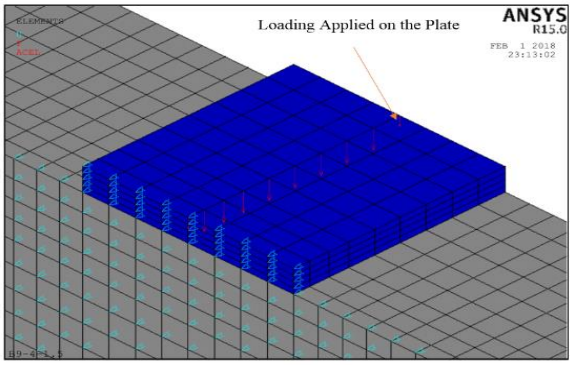

Fig.12: Load applied on the plate

5. Results of nonlinear finite element models

The aim of the comparison of the results of FEM and the experimental is to ensure that the; elements type, material properties, real constants and convergence criteria are adequate to model the response of the member.

5.1 Camber due to prestressing force

Figure 13 show the camber due to prestressing force that obtained from the solution of nonlinear finite element models that varied from 0.2 mm to 1.1 mm. The camber values decreased by increasing the DSF compared with the corresponding control beams. In addition, the finite element model of B3, which contained 1% DSF and 60% PPR, demonstrated the smallest camber compared to all beams. The sample B9, which contained 1.5% DSF of the concrete volume and 90% PPR, showed the highest camper compared by all beams. Finally, all the previous confirmed that a direct proportionality between stiffer responses and the high ratios of DSF.

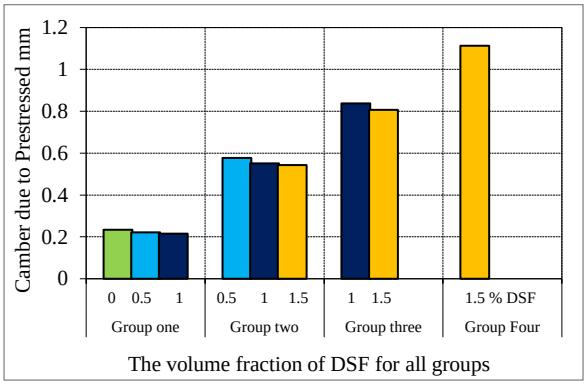

Fig. 13: Camber due to prestressed mm

5.2 Load deflection behavior

Figure 14 to 22 show deformed shape (D-shape) for all FEM beams. Figure 23 to 31 show the load-deflection curves (L-d curve) obtained from the experimental and finite element models for all beams. Table 6 and figures 32 and 33 show the comparison between the results of the experimental and FEM of cracking load and ultimate load respectively, for all samples. The ratio between the FEM to the experimental results of the cracking load varies from 0.89 to 1.30. The ratio between the FEM to the experimental results of the ultimate load varied from 1 to 1.05. From the previous figure and table 6 show the cracking load and ultimate load for all models contained DSF were higher than the corresponding control beams. Also, the FEM cracking load and ultimate load improve by increasing DSF and PPR. The sample B9, consist of 1.5% DSF of the concrete volume and 90% PPR, showed the highest numerical cracking load and ultimate load compared by all FEM. Finally, there is an agreement between the numerical and experimental results for the illustrated beams. This agreement indicates that the constitutive models used for concrete and reinforcement can capture the fracture behavior for a certain level of adequacy. It can be also noted from the figures that all models which contained DSF exhibited higher post-cracking stiffness responses and smaller deflections at the same value of load when compared to corresponding control beams. This may be attributed to the higher tensile strength and better post-cracking behavior of steel fiber concrete, which resulted in higher tension stiffening and less curvature of the cross section of the finite element models.

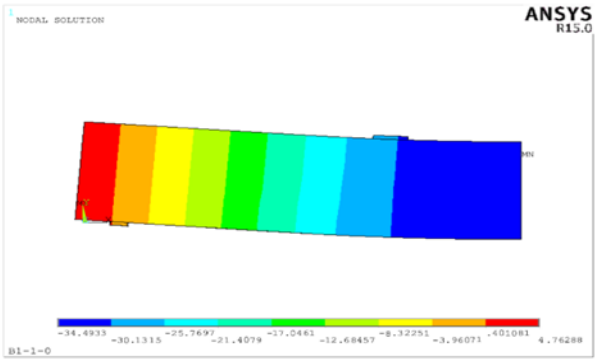

Fig. 14: D-shape, B1 in group one, without DSF

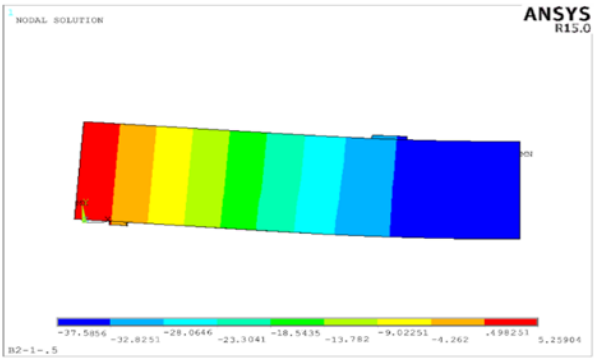

Fig.15: D-shape, B2 in group one, with 0.5% DSF

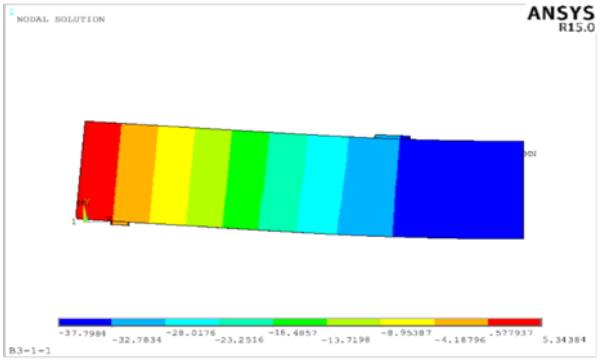

Fig. 16: D-shape, B3 in group one, with 1% DSF

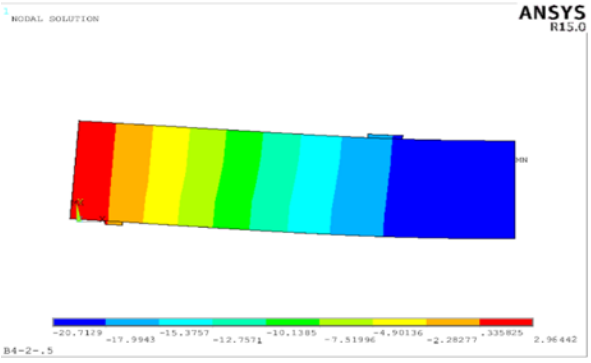

Fig.17: D-shape, B4 in group two, with 0.5% DSF

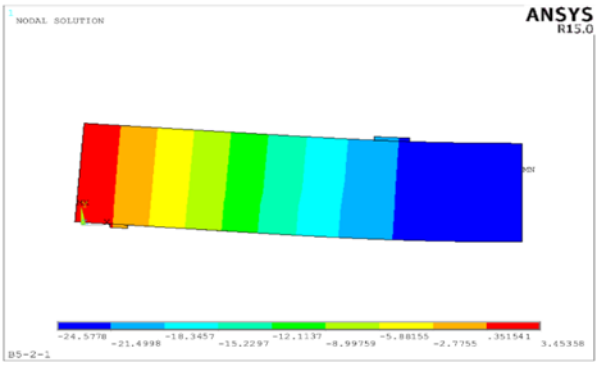

Fig.18: D-shape, B5 in group two, with 1% DSF

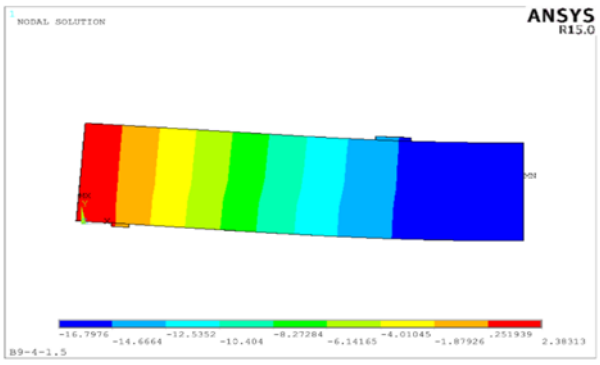

Fig. 22: D-shape, B9 in group four, with 1.5% DSF

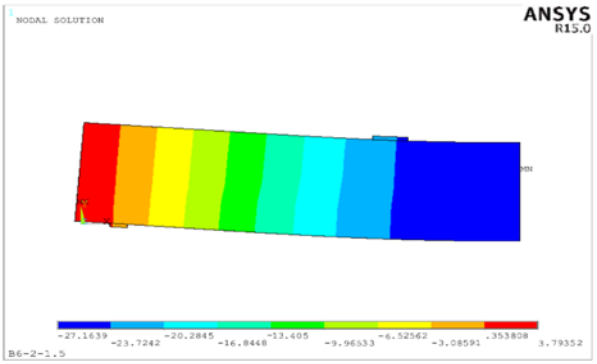

Fig.19: D-shape, B6 in group two, with 1.5%DSF

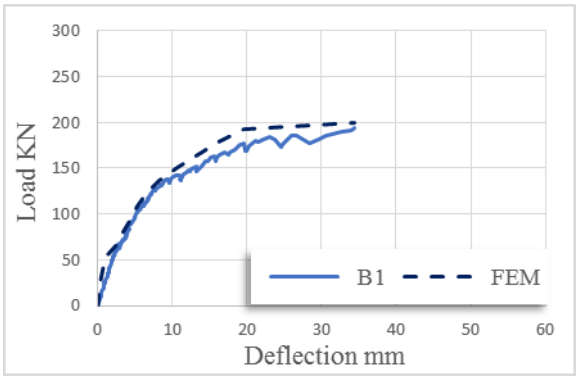

Fig.23: L-d curve, B1 in group one, without DSF

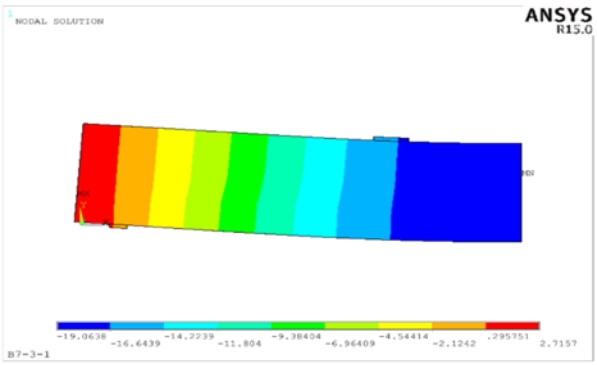

Fig.20: D-shape, B7 in group three, with 1%DSF

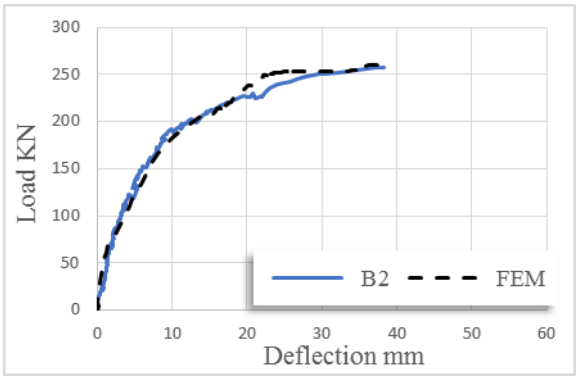

Fig.24: L-d curve, B2 in group one, with 0.5% DSF

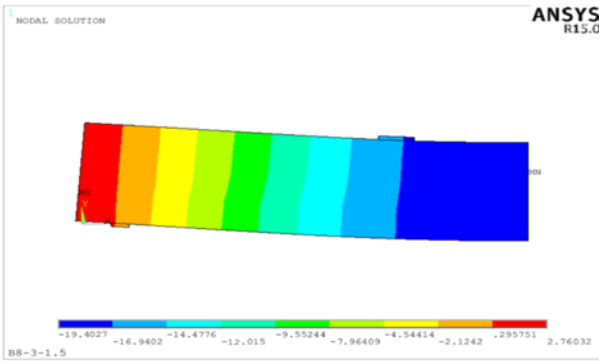

Fig.21: D-shape, B8 in group three, with 1.5%DSF

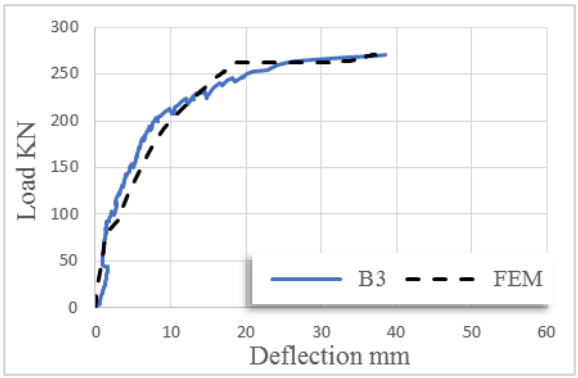

Fig.25: L-d curve, B3 in group one, with 1% DSF

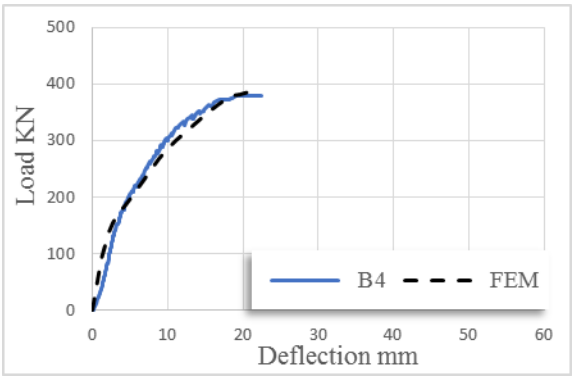

Fig.26: L-d curve, B4 in group two, with 0.5% DSF

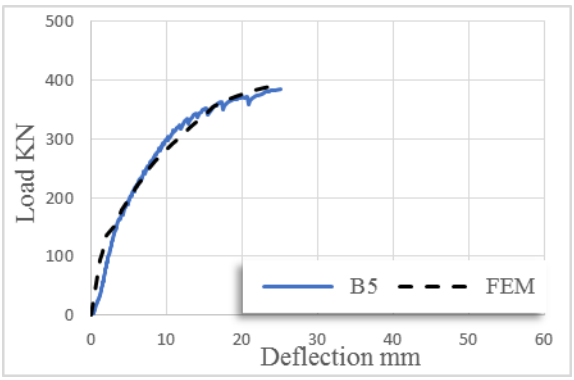

Fig.27: L-d curve, B5 in group two, with 1% DSF

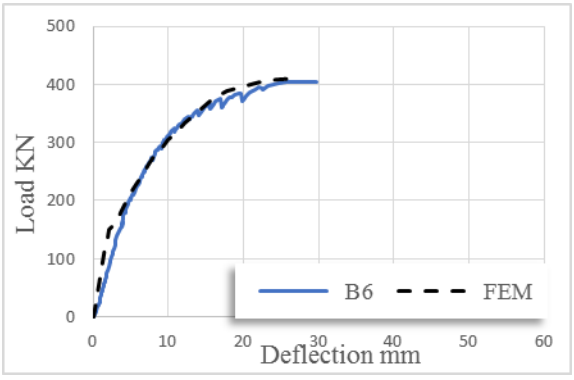

Fig.28: L-d curve, B6 in group two, with 1.5% DSF

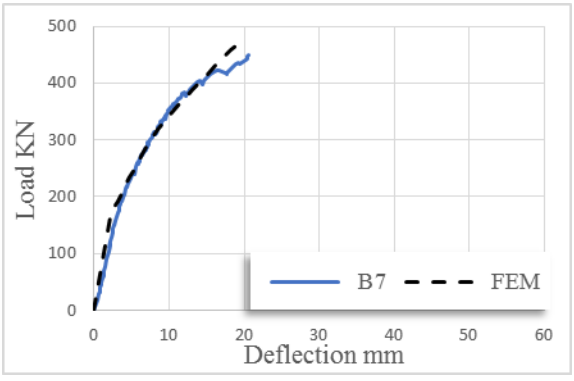

Fig.29: L-d curve, B7 in group three, with 1% DSF

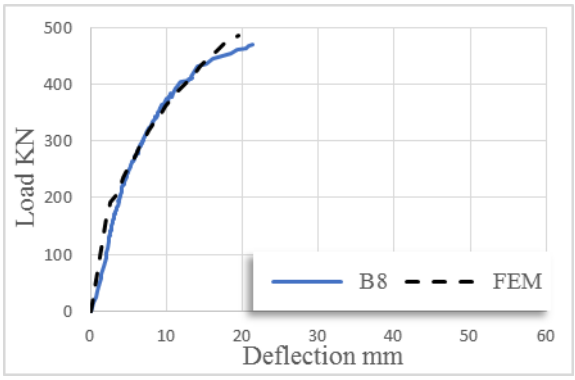

Fig.30: L-d curve, B8 in group three, with 1.5% DSF

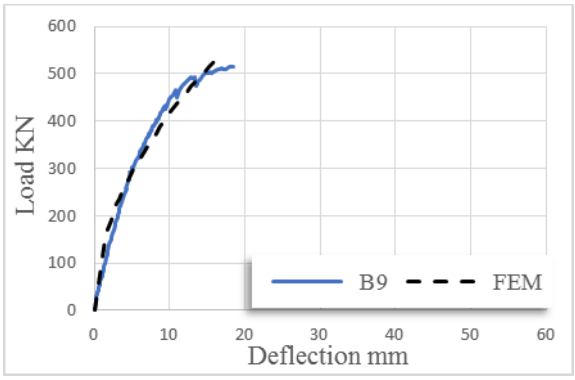

Fig. 31: L-d curve, B9 in group four, with 1.5% DSF

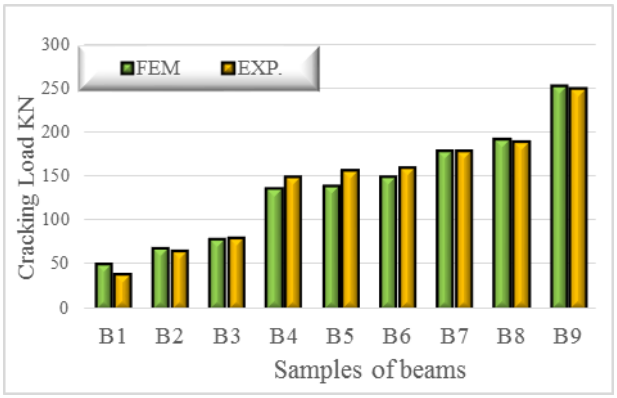

Fig. 32: Cracking load comparison between FEM and EXP.

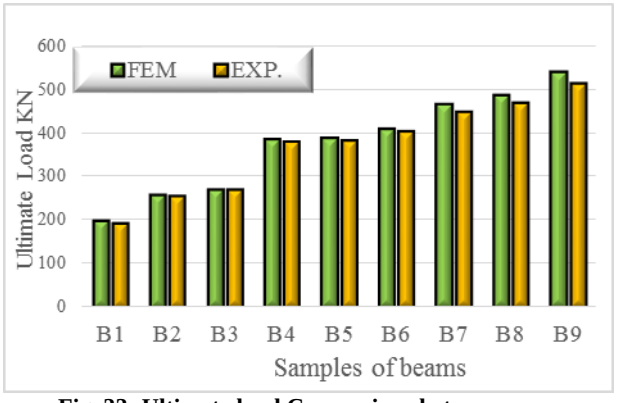

Fig. 33: Ultimate load Comparison between FEM and EXP.

Table 6: Experimental and FEM of cracking load, Yielding load and Ultimate load

Beams ID	Cracking Load (KN)			Yielding Load (KN)			Ultimate Load (KN)		
	FEM	EXP	FEM/EXP	FEM	EXP	FEM/EXP	FEM	EXP	FEM/EXP
B1	52	40	1.30	122.1	120.7	1.01	200	193.67	1.03
B2	70	67	1.04	166	158.7	1.05	260	257.39	1.01
B3	80	82	0.98	178.2	178.3	1	270	270.27	1.00
B4	137	150	0.91	251.7	269.9	0.93	386	379.93	1.02
B5	140	157	0.89	262.3	274.1	0.96	390	383.74	1.02
B6	150	160	0.94	276.3	290.4	0.95	410	404.13	1.01
B7	179	180	0.99	318.4	317.8	1	468	448.41	1.04
B8	193	190	1.02	332.6	338.3	0.98	486	468.90	1.04
B9	253	250	0.94	416.5	403.5	1.03	540	514.81	1.05

3.5 Tensile steel strain behavior

Experimental strain data, the control and fibrous beams, were measured from strain gauges at the mid-span of non-prestressed steel bar. Figure 34 to 42 show tensile steel strain curves (T-Strain) for all beams. Table 6 and figure 43 show the comparison between the results of the experimental and FEM of yielding load for all samples. The ratio between the FEM to the experimental results of the yielding load varies from 0.93 to 1.05. The table shows the yielding load for all models contained DSF were higher than the corresponding control beams. Also, the FEM of yielding load improve by increasing DSF and PPR. Comparing the load-strain plots from the finite element analyses with the experimental data for the flexural non-prestressed reinforcing at mid-span for each beam, it can be noted that, all beams show good agreement for the strains of the finite element analysis with the experimental results.

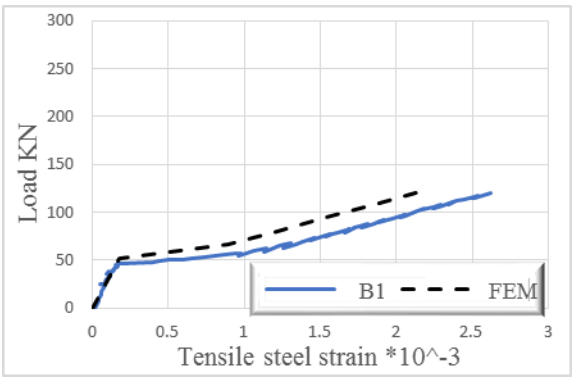

Fig.34: T-Strain, B1 in group one, without DSF

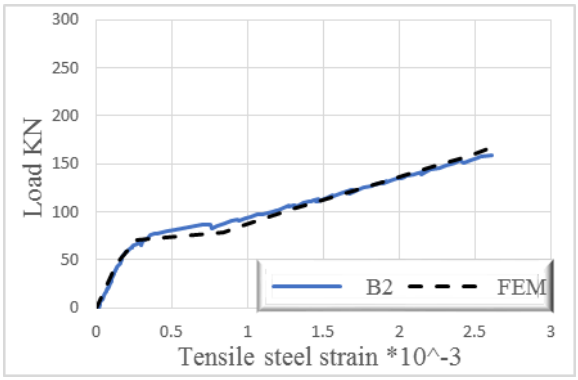

Fig.35: T-Strain, B2 in group one, with 0.5% DSF

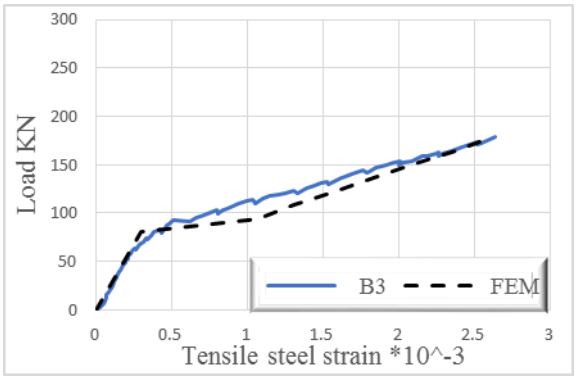

Fig.36: T-Strain, B3 in group one, with 1% DSF

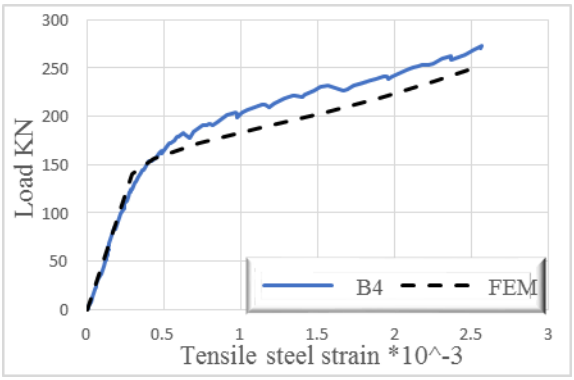

Fig.37: T-Strain, B4 in group two, with 0.5% DSF

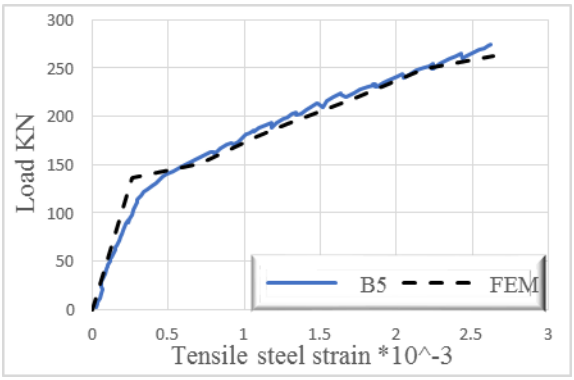

Fig.38: T-Strain, B5 in group two, with 1% DSF

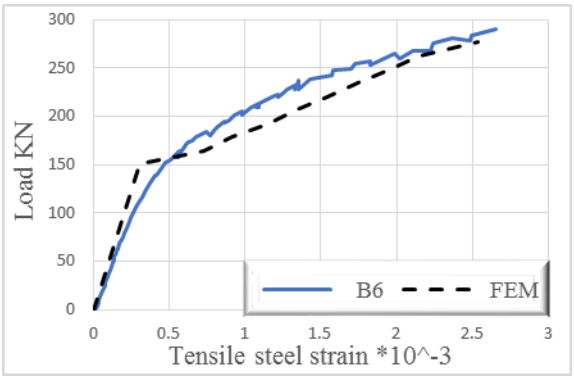

Fig.39: T-Strain, B6 in group two, with 1.5% DSF

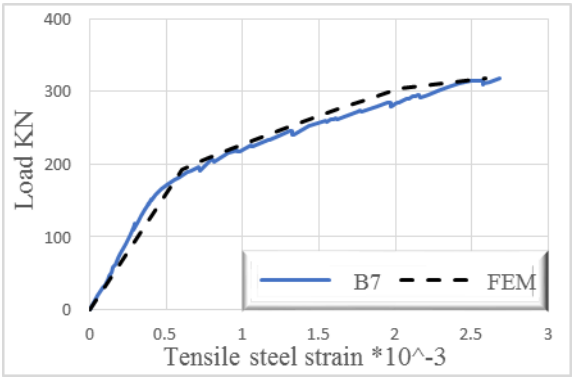

Fig.40: T-Strain, B7 in group three, with 1% DSF

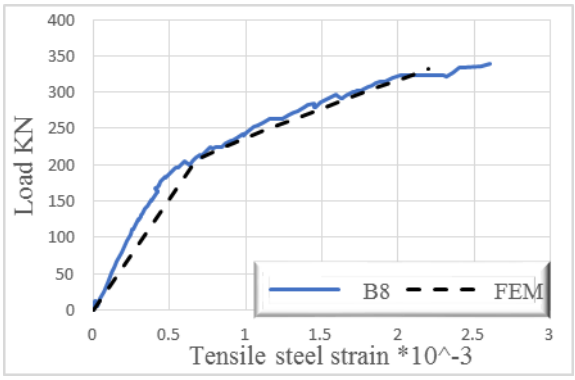

Fig.41: T-Strain, B8 in group three, with 1.5% DSF

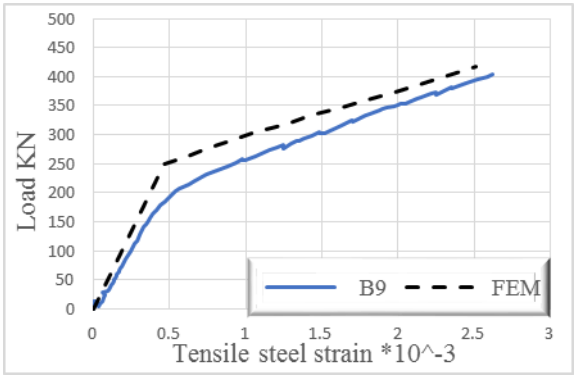

Fig.42: T-Strain, B9 in group four, with 1.5% DSF

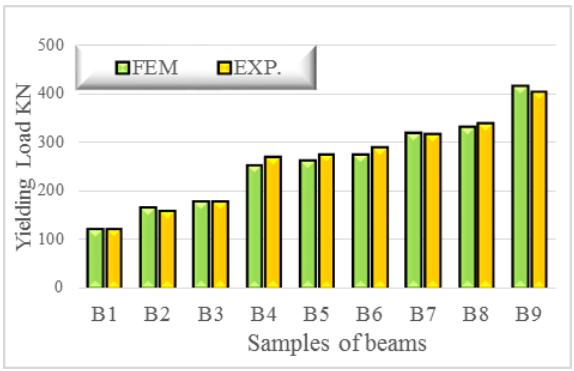

Fig. 43: Yielding load comparison between FEM and EXP.

6. Conclusions

From this research, the following conclusions can be reached;

- The camber due to prestressing force that obtained from the solution of nonlinear finite element models that varied from 0.2 mm to 1.1 mm. The camber values decreased by increasing the DSF compared with the corresponding control beams.
- The ratio between the FEM to the experimental results of the cracking load varies from 0.89 to 1.30. The ratio between the FEM to the experimental results of the ultimate load varied from 1 to 1.05. The cracking load and ultimate load for all models contained DSF

were higher than the corresponding control beams. Also, the FEM cracking load and ultimate load improve by increasing DSF and PPR. The sample B9, consist of 1.5% DSF of the concrete volume and 90% PPR, showed the highest numerical cracking load and ultimate load compared by all FEM.

- The ratio between the FEM to the experimental results of the yielding load varies from 0.93 to 1.05. All models contained DSF were higher than the corresponding control beams. Also, the FEM of yielding load improve by increasing DSF and PPR.

- Finally, the results that obtained by using a numerical finite element models by using ANSYSv15 program show an agreement between the numerical and experimental results for the illustrated beams. This agreement indicates that the constitutive models used for concrete and reinforcement can capture the fracture behavior for a certain level of adequacy. On the other hand, all models which contained DSF exhibited higher post-cracking stiffness responses and smaller deflections at the same value of load when compared to corresponding control beams. This may be attributed to the higher tensile strength and better post-cracking behavior of DSF concrete, which resulted in higher tension stiffening and less curvature of the cross section of the finite element models.

REFERENCES

1. Hayder Qais Majeed," Nonlinear finite element analysis of steel fiber reinforced concrete deep beams with and without opening", Journal of Engineering, Vol.18, 2012.
2. Lawrance KL, "ANSYS Tutorial Release 7.0 and 6.1", SDC Publications, Canonsburg, 2002.
3. Barbosa AF, Riberio GO, "Analysis of reinforced concrete structures using ANSYS nonlinear concrete model", Computer. Mech, pp. 1-7, 2004.
4. Edward G. Nawy,"Prestressed concrete",Fifth edithion,Printice Hall,2010.
5. Mashhour Ghoneim and Mahmoud El-Mihilmy,"Design of reinforced concrete structures",First Edition,2008.
6. Arthur H. Nilson,"Design of prestressed concrete", Second edition, Puplishe by John Wiley and Sons, 1987.
7. M.A.M. El Zareef, "conceptual and structural design of buildings made of lightweight and infra-lightweight concrete", Msc. Thesis, Von der Faculty VI–Planen Bauen Umwelt der Technischen University, Berlin, 2010.
8. Nicolas Ali Libre et.al," Mechanical properties of hybrid fiber reinforced lightweight aggregate concrete made with natural pumice", Construction and Building Materials, Vol. 25, pp. 2458–2464, 2011.
9. BS 5328 Part 1: 1991, "Part 1. Guide to specifying concrete".
10. ACI 213 R-87, "Guide for structural lightweight aggregate concrete", Rep. by ACI Committee, 1999.
11. Oğuz AkNn Düzgün, Rüstem Gül and Abdulkadir Cüneyt Aydin "Effect of steel fibers on the mechanical properties of natural lightweight aggregate concrete", Materials Letters, Vol. 59, pp. 3357– 3363, 2005.
12. ACI 544.1R-96," State-of-the-Art Report on Fiber Reinforced Concrete".
13. Mahmoud Hassanpour, Payam Shafigh and Hilmi bin Mahmud," Light weight aggregate concrete fiber reinforcement – A review", Construction and Building Materials, Vol. 37, pp. 452–461, 2012.
14. Hemant B. Dhonde, Y.L. Mo and Thomas T.C. Hsu," Fiber Reinforcement in Prestressed Concrete Beams", Texas department of transportation and the federal highway administration project 0-4819,2005.
15. Leonharadt, " Discussion of: Strength and behavior of deep beams in shear", Proceedings of the American Society of Civil Engineers, Vol.92, 1972.
16. O.F. Hussien et. al, " Behavior of bonded and unbonded prestressed normal and high strength concrete beams", Housing and Building National Research, Vol. 8, PP.239-251,2012.
17. ESS 4756-1 / 2007, Egyptian standard specification, "Cement-physical and mechanical tests".
18. Egyptian Code No. 203/2007.
19. F.A. Tavarez, "Simulation of behavior of composite grid reinforced concrete beams using explicit finite element methods", Master of science thesis, University of Wisconsin–Madison, Madison, Wisconsin, 2001.
20. ANSYS, (2015), Release 14.0 Documentation. ANSYS Inc., http://www.ansys.com.

21. Willam, K.J. and Warnke, “Constitutive Model for Triaxial Behaviour of Concrete,” Seminar on Concrete Structures Subjected to Triaxial Stresses, International Association of Bridge and Structural Engineering Conference, Bergamo, Italy, p.174, 1974.
22. Randa F. Hegazi, " Modeling of lightweight concrete elements using nonlinear finite element analysis", Msc. Thesis, Faculty of Engineering-Ain Shams University, 2016.
23. Jianming Gao, Wei Suqa & Keiji Morino," Mechanical Properties of Steel Fiber-reinforced, High-strength, Lightweight Concrete",Cement and Concrete Composites, Vol. 19, pp. 307–313, 1997.
24. Anthony J. Wolanski, B.S.," Flexural behavior of reinforced and prestressed concrete beams using finite element analysis", Msc. Thesis, Faculty of the Graduate School, Marquette University, the U.S. state, 2004.
25. Kachlakev, D.I., etal, “Finite Element Modeling of reinforced concrete structures strengthened with frp laminates,” California Polytechnic State University, San Luis Obispo, CA and Oregon State University, Corvallis, OR for Oregon Department of Transportation, 2001.

24/6/2018